Parametric study of ion acceleration in a one-dimensional plasma expansion using the particle-in-cell simulation

Tudor Nedelea and Herbert M. Urbassek*
Fachbereich Physik, Universität Kaiserslautern, Erwin-Schrödinger-Straße, D-67663 Kaiserslautern, Germany
(Received 19 November 2003; published 24 May 2004)

The one-dimensional expansion of a plasma off a planar wall into a vacuum is studied using particle-in-cell computer simulation. Particular emphasis is put on the acceleration of ions in the plasma. Energy transfer from the electronic to the ionic subsystem, the energy spectra of the ions, and the center-of-mass motion of the ion cloud are monitored. Various parameters that influence the acceleration process are studied: the presence of several ion charge states, of neutrals, the effects of a binary mixture of ions, and of a thermal nonequilibrium between ions and electrons.

DOI: 10.1103/PhysRevE.69.056408 PACS number(s): 52.38.Kd, 52.65.Rr, 52.38.Mf

I. INTRODUCTION

After laser ablation off a surface, a plasma cloud forms in front of the surface and expands into the vacuum above it [1–3]. This basic phenomenon of plasma expansion has raised the interest of researchers as soon as the first laser ablation experiments have been performed [4]. Measurements—taken both with nanosecond [2,5,6] and femtosecond-laser [7,8] pulses—show that the energy distribution of the ions in the expanding plasma cloud extends to surprisingly high energies, and may reach several 100 or 1000 eV. In other words, they may reach values that are a factor of 100 or 1000 larger than the equivalent of reasonable material surface temperatures, e.g., the boiling or critical temperature.

Theoretical analyses of the expansion process are often based on a hydrodynamic modeling, in which assumptions on the equilibrium nature of the process enter. Only in the last decade, numerical efforts have become more widespread, often, however, with an emphasis on modeling the particular situations encountered in a specialized experiment without a general analysis. We note, however, that already the early kinetic analysis of Gurevich *et al.* [9] was able to show the existence of electrostatic acceleration mechanisms in the expanding flow, and could hence demonstrate that these mechanisms are able to accelerate ions up to the initial electron velocity; we also note another early simulation [10] which exemplified the role of the expansion-front space-charge field.

Very recently, the well-known particle-in-cell (PIC) computer simulation algorithm [11–13] was applied to study specific aspects of the plasma-expansion dynamics [14,15]. It allowed to monitor ion and electron distribution functions during the early phases of plasma expansion. By the self-consistent calculation of the time-varying shape of the ion and electron clouds, as well as the space-charge generated electrical field, a detailed analysis of the ion acceleration mechanism and the conversion of electron thermal energy to directed ion energy became possible.

These previous simulations [14,15] treated a strongly idealized model situation: The plasma is assumed to be fully ionized, and to contain only a single ion species in the singly ionized charge state. These idealized conditions allowed quite a general analysis of this model problem since by the introduction of scaled variables a complete numerical solution of this problem could be obtained. However, the conditions in a realistic plasma-expansion experiment may deviate in several respects from the idealized assumptions of the previous investigations. In the present paper, we therefore want to relax these strict assumptions and introduce various plasma processes during the expansion process into our simulation: the presence of two ion charge states, the emission of two ion species with different masses, the effect of collisions with neutrals, and, finally, we allow for the electron component to possess a higher kinetic energy upon emission off the surface than the ion species. By considering each of these processes one at a time, and by comparing the results to those of the idealized simulation (as a reference case) it will be possible to trace—at least qualitatively—the influence of various plasma processes on the expansion dynamics. Our interest shall focus on the energy conversion from the electronic to the ionic system and the concomitant processes leading to ion acceleration during expansion. Of particular interest will be the preferential acceleration mechanisms operating in systems containing different ion species or charge states.

Our results may be used to discuss available data on ion energy distributions measured in expanding laser-induced plasmas. However, a comparison to these data must of necessity be of a qualitative nature, due to several restrictions in our model.

(i) Due to computer time restrictions, our simulations extend only to a time up to $(4-12)\tau$ after ablation, where τ denotes the laser pulse length. Thus our results are restricted to the early phases of expansion, and hence to the processes occurring in the vicinity of the ablating wall. In experiment, data are however taken usually far away from the wall and at later times.

(ii) Laser interaction with the expanding plasma offers an important channel to heat the plasma and to allow for ion acceleration to high energies. While this process can in prin-

*Electronic address: urbassek@rhrk.uni-kl.de; URL: http://www.physik.uni-kl.de/urbassek/

ciple be included in the simulation [16,17] we did not attempt to do so in the present stage of investigations. This feature makes our simulations applicable in particular to ultrafast laser ablation on the picosecond or femtosecond time scale, where laser heating of the plasma will be of minor importance [18].

(iii) In any realistic plasma, a multitude of collisional processes will be operative simultaneously; we mention the (three-body, radiative, and dielectronic) recombination, collisional excitation and ionization processes, elastic and charge-exchange collision processes, and radiative energy loss by bremsstrahlung [1,2,19,20]. The importance of each of these processes needs to be assessed for the particular experiment to be described, while we wish to study the generic physics of ion acceleration in an expanding plasma, rather than simulate a specific experiment.

II. SYSTEM AND SIMULATION

A total number of N_0 singly charged ions (mass M, charge $+e$) and of N_0 electrons (mass m, charge $-e$) are desorbed from a planar surface between time $t=0$ and τ. To be specific, all simulation results will be presented for the case of Al ($M=27.0$ amu), i.e., $M/m \cong 4.9\times 10^4$. Before and after this period of time, no desorption takes place, while during this time the desorption flux is constant. We assume the electron and ion current densities to be of the same magnitude J in order to leave the ablation target electrically neutral. We furthermore assume that the phase space density $f_0(x=0,v,t)$ of the ions immediately after desorption outside the surface is given by the half-Maxwellian distribution

$$f_0(x=0,v,t) = n_0 \sqrt{\frac{2M}{\pi k_B T_0}} \exp\left(-\frac{Mv^2}{2k_B T_0}\right), \quad v>0, \quad (1)$$

for $0<t<\tau$. Here v is the velocity perpendicular to the surface. Furthermore, T_0 is the surface temperature, k_B is Boltzmann's constant, and n_0 is the number density of ions immediately outside the surface. We note that the average ion velocity in the direction perpendicular to the surface is $v_0=\sqrt{2k_BT_0/\pi M}$, and it is $J=en_0v_0$. For the electrons we also assume a half-Maxwellian, i.e., thermal, emission distribution with identical temperature T_0.

Since the ablation target does not charge up, its electrical potential Φ stays constant; thus we may set $\Phi(x=0)=0$ at all times. This means in particular that we assume all particles that return to the surface to reflect from it.

We employ the PIC algorithm [11–13] to solve the coupled plasma-expansion problem formulated above. Technical details of the application of this code to the plasma emission and expansion problem have been published elsewhere [14,15]. The simulations follow the plasma expansion up to time $t=4\tau$.

III. RESULTS

A. Reference case

As a reference case, we present the simulation results obtained for the expansion of a fully ionized plasma with parameters as given in Sec. II. In particular, the plasma consists of a single ion species, in its singly ionized charge state; the electron and ion temperatures upon emission from the surface are equal, $T_e=T_i=T_0$. Emission lasts for a period $\tau=10t_i$, where $t_i=\sqrt{M\varepsilon_0/n_0e^2}$ is the ion plasma period. We follow plasma expansion up to a time 4τ. This system has been intensively studied in the past [14,15].

Figure 1 summarizes the main characteristics of the system. In Fig. 1(a), we display the time evolution of the (normalized) energies in the system. To define these, we start with the energy conservation

$$\sum_\nu E_\nu(t) + E_{\text{field}}(t) = k_B T_0 \sum_\nu N_\nu(t), \quad (2)$$

where ν indicates the particle species (e, electrons; i, ions), and $N_\nu(t)$ and $E_\nu(t)$ denote the number and kinetical energy (in flow direction away from the surface), respectively, of particles of species ν at time t. The potential energy of the field, E_{field}, is given by

$$E_{\text{field}} = \frac{1}{2}\int \rho(x)\Phi(x)dx, \quad (3)$$

where $\rho(x)$ is the space-charge density and $\Phi(x)$ is the potential at point x. Equation (2) has its origin in the fact that no energy is lost in the system, while each particle that enters the system by emission from the wall introduces on the average an energy k_BT_0 in flow direction. Introducing the normalized energies per particle

$$\epsilon_\nu = \frac{1}{k_BT_0}\frac{E_\nu}{N_\nu} \quad (4)$$

and the normalized field energy

$$\epsilon_{\text{field}} = \frac{1}{k_BT_0}\frac{E_{\text{field}}}{\sum_\nu N_\nu}, \quad (5)$$

the energy balance, Eq. (2), then reads

$$\frac{\sum_\nu \epsilon_\nu N_\nu}{\sum_\nu N_\nu} + \epsilon_{\text{field}} = \epsilon_{\text{tot}}. \quad (6)$$

This defines the (normalized) total energy ϵ_{tot}. Energy conservation, Eq. (2), predicts $\epsilon_{\text{tot}}=1$. Figure 1(a) proves that our simulation well fulfills this criterion.

We observe that at the end of the emission phase, $t=\tau$, electrons have transferred a considerable part of their energy to the ions. Later on they transfer almost all their remaining energy to the ions. This constitutes the energy source for ion acceleration. Figure 1(b) displays the ion density $n_i(x)$ at the end of the emission phase $t=\tau$ and at $t=4\tau$. At $t=\tau$, an exponentially decreasing density profile is observed with a relatively sharply defined ion front at $x\cong 6v_0\tau$. After the emission phase, the ion cloud separates from the wall and expands into vacuum. Figure 1(c) displays the motion of the center of mass of the cloud into vacuum. The dynamics of

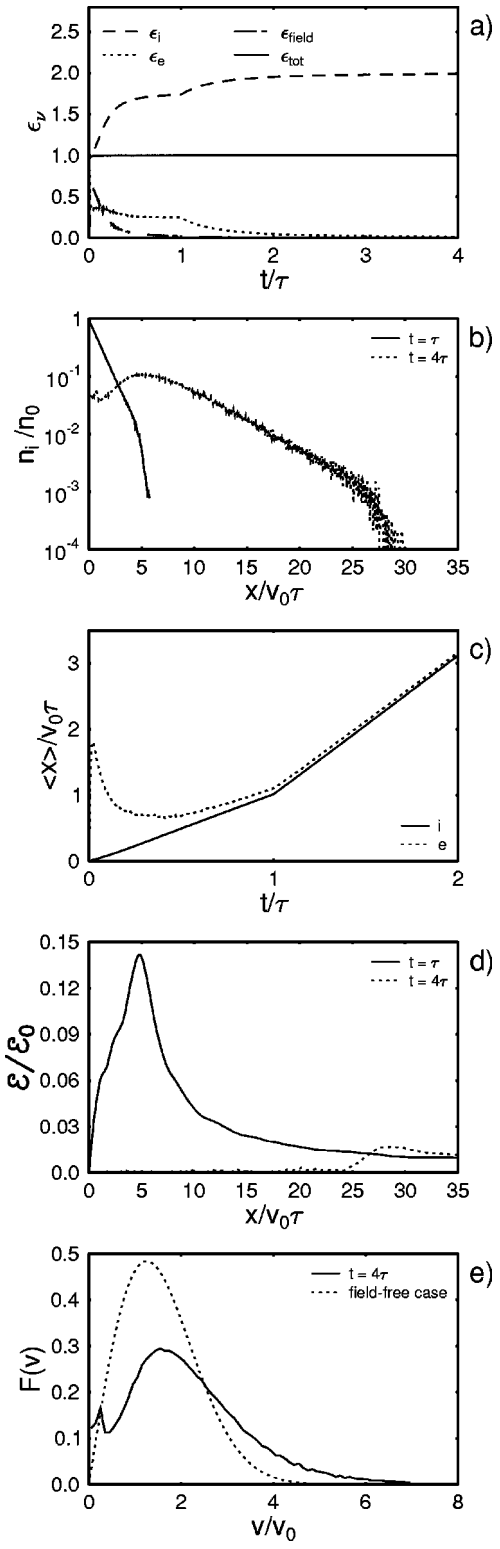

FIG. 1. Characteristics of the reference simulation. (a) Time evolution of normalized energy per particle, Eq. (4). (b) Ion density distribution at times $t=\tau$ and $t=4\tau$. (c) Time evolution of the position of the centers of mass $\langle x(t)\rangle$ of the ion and electron clouds. (d) Space dependence of the electrical field at times $t=\tau$ and $t=4\tau$. (e) Ion velocity distribution, Eq. (9), at time $t=4\tau$ compared to the field-free case.

the center of the electron cloud is included as well. Electrons initially move with high speed into vacuum until they are forced back by the electrostatic field developing between the separated ion and electron clouds. Then a quasineutral plasma develops, in which the center of the electron and ion clouds jointly move away from the surface. Note the change in slope at time $t=\tau$. It is not an artifact of the simulation, but results from the fact that the mass of the cloud continually grows until time $t=\tau$, and then stays constant.

Figure 1(d) shows the electrical field $\mathcal{E}$ above the wall at the end of the emission phase, $t=\tau$, and at $t=4\tau$. We use as unit of the field

$$\mathcal{E}_0 = \frac{\Phi_0}{\lambda_D} = \frac{2}{\pi}\sqrt{\frac{k_B T_0 n_0}{\epsilon_0}}, \tag{7}$$

where

$$\Phi_0 = \frac{2kT_0}{\pi e} \tag{8}$$

and $\lambda = \sqrt{\epsilon_0 kT_0/n_0 e^2}$ is the Debye length of the system. An estimate of the electrical field may be derived from a self-similar hydrodynamic model [15,21]. For the parameters of our plasma, it predicts a field maximum of $\mathcal{E}(t=\tau)=0.1\mathcal{E}_0$, in fair agreement with the simulation.

Note that the field maximum occurs at the location of the ion front, $x\cong 6v_0\tau$. At later times, the field has almost vanished within the expanding plasma cloud and has survived only at the location of the ion front, i.e., $x\cong 28v_0\tau$ at time $t=4\tau$.

Finally, Fig. 1(e) presents the velocity distribution of the ions at time $t=4\tau$. We define it as

$$F(v,t) = \int f(x,v,t)dx \tag{9}$$

and normalize it to $\int F(v,t)dv=1$. It measures the velocity distribution of ions averaged throughout the simulation volume at this time. In order to characterize the acceleration process, we compare the distribution to the velocity distribution as obtained by a field-free flow, which applies, when the action of all electrical fields is disregarded. With the emission distribution, Eq. (1), it is

$$F_0(v) = v\tau f_0(x=0,v,t) \tag{10}$$

for $t\geqslant\tau$. Due to the absence of fields, F_0 does not change in time after emission.

It is observed that already at this early time, considerable ion acceleration has occurred, such that the population of high-energy ions, which are in the (front of the) plasma cloud, is strongly enhanced. Certainly, for times $t>4\tau$, further ion acceleration will happen at the ion front [9].

B. Two ion charge states

In this simulation, we consider the ion cloud to consist of two charge states, a singly charged and a doubly charged ion species, denoted by indices 1 and 2, respectively. They are emitted from the wall with current densities J_1 and J_2, respectively. With the electron current J_0, it holds $J_1+J_2=J_0$ in

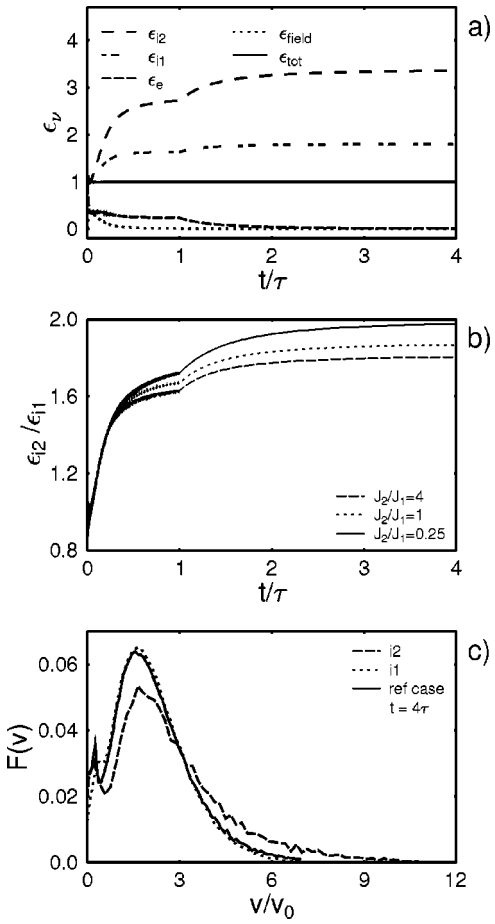

FIG. 2. Characteristics of an expansion containing two ion charge states. (a) Time evolution of normalized energy per particle, Eq. (4). (b) Time evolution of the ratio of the average energy of a doubly charged ion to a singly charged ion. The ratio of the emission currents J_2/J_1 serves as parameter. (c) Ion velocity distribution, Eq. (9), at time $t=4\tau$, compared to the reference case.

order to guarantee electrical neutrality of the expanding plasma. In this particular simulation, we choose $J_1=J_2$, i.e., double as many singly ionized ions are emitted as doubly ionized ions.

Figure 2(a) shows the time evolution of the particle and field energies in the system. We observe that the field energy and the electron energy decay to zero on similar time scales as in the reference case, Fig. 1(a). But furthermore, we observe that the energy is transferred considerably more efficiently into the doubly charged than into the singly charged ion system. The ratio of average ion energies at the end of the simulation amounts to $\epsilon_2/\epsilon_1=1.87$. We repeated the simulation for other values of the ion currents off the wall, cf. Fig. 2(b). For $J_2/J_1=4$ (1/4) we found $\epsilon_2/\epsilon_1=1.80$ (198). This is a moderate dependence, which, however, indicates that a dilute doubly charged species is more efficiently accelerated.

Figure 2(c) displays the velocity distribution. While singly charged ions follow closely the reference case, doubly charged ions show a strong enhancement in the population of energetic ions. These now extend up to velocities $>9v_0$.

We conclude that the acceleration of doubly charged ions is considerably more pronounced than that of singly charged ions. This is a consequence of the action of the space-charge field, which couples more strongly to the doubly charged ions. We note that such a charge segregation in expanding plasmas, where highly charged ions attain higher energies than low-charged ions, has already been found in very early experimental investigations on laser-induced plasmas [22,23] but continues until today to be a subject of intense experimental research [5,25,24].

C. Different ion species

In this simulation, we study the ablation of a stoichiometric mixture of a heavy (h) and a light (ℓ) species with masses $M_h=107.9$ amu and $M_\ell=10.8$ amu, respectively. The ion masses were chosen to be those of silver and boron, respectively, with a mass ratio of $M_h/M_\ell\cong 10$. The emission currents are chosen equal, $J_h=J_\ell$, such that equal amounts of species h and species ℓ are emitted.

Figure 3(a) shows the average particle and field energies. We see that the light species is considerably more strongly accelerated than the heavy species, and at time $t=4\tau$, it is $\epsilon_\ell/\epsilon_h=1.98$.

The origin of this preferential acceleration can be seen by comparing Figs. 3(b) and 3(d). Figure 3(b) displays the density distribution of light and heavy particles at the end of the emission phase, $t=\tau$. The ion front of the heavy species is at around $2.5v_0\tau$, while that of the light species is at $9.5v_0\tau$; that is, a factor of roughly 3.8 further expanded. This is mainly a consequence of the fact that at equal temperatures, the light species will have a $\sqrt{10}$ times larger velocity than the heavy species. But besides this rather trivial mass effect, these data also indicate a slight preferential acceleration of the light species, which we shall analyze further below.

In Fig. 3(c) we show the total ion charge density $n_\ell+n_h$ and compare it to the electron density n_e. The double-layer structure close to the expansion front at $x\cong 9v_0\tau$ is distinctly visible. Note, however, the strong curvature of the ion density at the position of the heavy-ion front, $x\cong 2v_0\tau$. Here, slight deviations from quasineutrality develop (barely visible in this scale), which will establish a space-charge field in this region.

The electrical field at time $t=\tau$, Fig. 3(d), shows a double-peak structure. The strongest maximum occurs in the region of the furthermost ion front, i.e., the front of the light particles. A second maximum has developed *within* the heavy-ion cloud, $x\cong 1v_0\tau$, while the field at the front of the heavy particles is, if anything at all, decreased. As a consequence, light particles are subject to a stronger field since they are situated closer to the overall expansion front. Note, however, that the field strengths are everywhere diminished with respect to that of the reference case, Fig. 1(d).

Figure 3(e) displays the normalized energy spectra $F(E)$ of the two particle species, which are obtained from the velocity spectra $F(v)$, Eq. (9), by

$$F(E)=F(v)\frac{1}{dE/dv}. \tag{11}$$

and normalizing to $\int F(E)dE=1$. Due to the initially strongly different velocities of the light and heavy ions, it is advisable

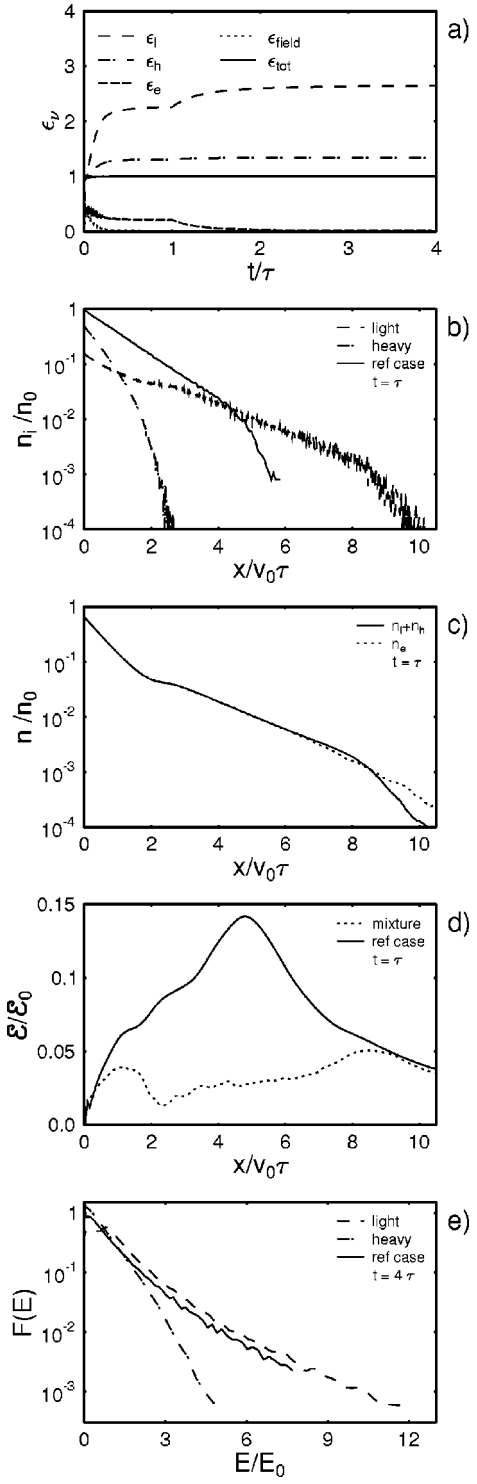

FIG. 3. Characteristics of the expansion of a plasma containing a mixture of a light (ℓ) and a heavy (h) ion species. (a) Time evolution of normalized energy per particle, Eq. (4). (b) Space dependence of the light- and heavy-ion densities at time $t=\tau$, compared to the reference case, Fig. 1(b). (c) Space dependence of the total ion density $n_\ell+n_h$ compared to the electron density n_e at time $t=\tau$. (d) Space dependence of electrical field at time $t=\tau$, compared to the reference case. (e) Energy distributions of light and heavy ions at time $t=4\tau$, Eq. (11), compared to the reference case.

to study *energy* rather than velocity spectra. This figure clearly shows the preferential acceleration of light particles at the expense of heavy particles. Light particles are found at high energies, $E\cong 5E_0$, with more than one order of magnitude higher probability than heavy particles.

In summary, the coupled expansion of two ion species with different masses in a plasma shows quite a complex behavior. For isothermal emission, the light ions have a higher velocity and are hence situated at the expansion front. Since the accelerating space-charge field is strongest here, the light species is preferentially accelerated. We note that experiments on plasma expansion of such two-component systems have been performed; such systems can be studied by laser ablation of compound targets. These experiments find indeed that the *velocity* of the lighter species is larger than that of the heavy species; however, the *energy* is not: Thus, for example, in an experiment [26] on the nanosecond-laser ablation of binary WCu targets, the average velocities v_i for $i=$Cu, W have been measured and $v_{\mathrm{Cu}}/v_{\mathrm{W}}=1.4$ has been found, corresponding to a ratio of average kinetic energies of $E_{\mathrm{Cu}}/E_{\mathrm{W}}=0.7$. It seems that frictionlike collision processes, which tend to assimilate the *velocities* of the various particle species, are decisive to understand these experimental results. The effect of collisions will hence be discussed in Sec. III D.

D. Collisions with neutrals

In this simulation we assume that apart from ions and electrons, also neutrals (n) are emitted from the wall at the same temperature T_0. We assume $J_e=J_i=J_n$. In order to couple neutrals to the charged species, we introduce elastic ion-neutral collisions. Collisions between ions and neutrals are treated using the PIC/Monte Carlo concept [13] while collisions among neutrals are ignored. The cross section is chosen in accordance with Ref. [27] as a (roughly) energy-independent hard-sphere cross section. In our approach, where times are scaled with τ, velocities with v_0, and the ion density with n_0, the cross section σ is chosen such that $n_0\sigma v_0\tau=1.14$. For computational reasons we perform the simulation only until time $t=2\tau$, until which time particles have performed on the average 5.4 collisions.

Figure 4(a) gives the time evolution of the energy per particle. The total energy now has risen to the value of $\epsilon_{\mathrm{tot}}=2$ (in comparison to $\epsilon_{\mathrm{tot}}=1$ in the reference case), since now the lateral degrees of freedom—with an average energy of $1k_BT_0$ for each particle—have to be included. As in the reference case, we observe a quick energy transfer from electrons to ions. Additionally a slow energy transfer from the ionic species to the neutrals can be seen. A closer inspection shows that the energies perpendicular to the flow of ions and neutrals are strongly coupled and decay identically. In flow direction, however, ions keep constantly accelerating by the electrical field. Part of this energy is transferred to the neutral system, but ions are always faster than neutrals and, as a consequence, ahead of neutrals. This feature is clearly shown in Fig. 4(b), where the centers of mass of the electronic, ionic, and neutral subsystems are shown. The change in slope visible at time $t=\tau$ has the same origin as described in

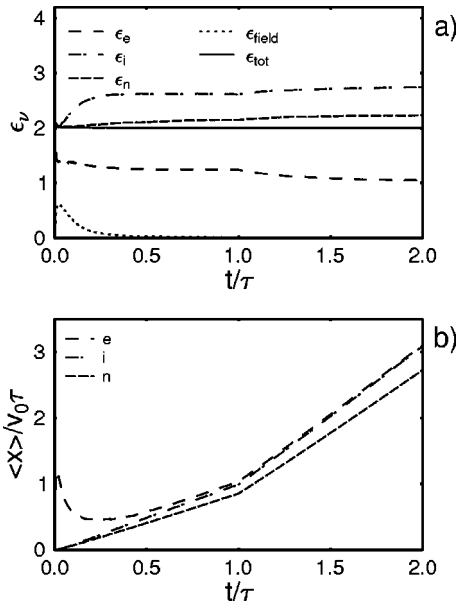

FIG. 4. Characteristics of plasma expansion including ion-neutral collisions. (a) Time evolution of normalized energy per particle, Eq. (4). (b) Time evolution of the position of the centers of mass $\langle x(t)\rangle$ of the ion, electron, and neutral clouds.

Fig. 1(c). Electrons and ions are strongly coupled by the electrostatic fields after this time. The coupling to the neutral system—while accelerating the neutrals, cf. Fig. 4(a)—is not strong enough to guarantee complete entrainment of the neutral cloud with the plasma such that, in the course of time, the neutral cloud lags behind the quasineutral plasma cloud.

We conclude that collisions between the ion and the neutral system introduce a sort of friction in the system, which decelerates ions and accelerates neutrals. It depends, of course, on the exact size of the collision cross section, to determine how strong any "velocity slip" between the ion and neutral species may develop. These processes, which will continue on time scales exceeding that of our simulation, have been explored previously with the help of hydrodynamic simulations [28].

Experiments in which the energy distributions of both neutrals and ions are measured are rare. An outstanding example is given in Ref. [29] on the laser ablation of a Cu target. Here it was found that the average energy of Cu^+ rises rapidly with the laser intensity; this finding is interpreted to result from the ambipolar acceleration of Cu^+ ions in the expanding plasma—in agreement with our analysis. At the same time, a moderate increase of the Cu^0 velocity with laser intensity is found and interpreted to be due to energy transfer from the ionic component to the neutral component. In addition to elastic collisions, the action of resonant charge exchange and three-body recombination collisions was postulated to aid in the energy transfer; these latter processes have been neglected in our model approach.

E. Hot electrons

We simulate a system, in which electrons are emitted with a temperature $T_{e,0}=100T_0$ off the wall. Such a situation might be realized in a strongly nonequilibrium ablation, such as in intense laser ablation processes, where electrons (which are directly energized by the laser light) may be emitted with considerably higher energies than ions. We note that the electron and ion energies upon emission, and even more so their distributions, are not available experimentally; hence our assumption of a half-Maxwellian distribution and a ratio of 1:100 of the ion to electron temperatures is meant as a model scenario in order to investigate the effects resulting from such a nonequilibrium emission distribution.

Figure 5(a) shows the time evolution of the average energies per particle. We see that in the long run, also here all electron energy is given to the ion system. The time needed for the transfer is, however, definitely longer than in the reference case. Therefore, we extended the simulation to $t=12\tau$ in order to get a complete picture of the events happening. In Fig. 5(b) we show the same quantities for the case where emission keeps going until time $t=4\tau$. At this time, electron and ion energies seem to have attained stationary values—electrons have kept only 20.3 % of their initial energy and transferred 79.0 % to the ion system, while the remainder still is stored in the potential energy of the field.

We also note that the field energy becomes quite huge; in the early phase of the expansion, it contains more than 60 % of the energy initially present in the system. This is a sign of a strong space-charge field acting as the means of ion acceleration.

Figure 5(c) shows the ion density distribution at time $t=\tau$. The position of the ion front has moved considerably out into vacuum to $x\cong 17v_0\tau$, evidencing the strong ion acceleration. Note, furthermore, that the exponential decay of the ion density in the reference case has changed to a rather broad plateau extending from $x\cong(4-15)v_0\tau$, while the ion density in the close vicinity of the surface shows a steep gradient. This density profile is the result of the ion equilibration with the quickly expanding fast electron cloud; in this process the ion cloud is stretched out into vacuum.

The space-charge field is shown in Fig. 5(d). It is considerably stronger than the field in the reference case. In order to include this field in the same plot as the reference field, we use the unit

$$\tilde{\mathcal{E}}_0=\frac{\tilde{\Phi}_0}{\lambda_D} \tag{12}$$

with

$$\tilde{\Phi}_0=\frac{2kT_{e,0}}{\pi e}, \tag{13}$$

that is, by replacing the ion temperature T_0 in Eq. (7) by $T_e=100T_{e,0}$; thus $\tilde{\mathcal{E}}_0=100\mathcal{E}_0$. Besides the overall strength of the field, three features deviate from the reference case: (i) Trivially, the position of the field maximum is shifted to larger distances, in agreement with the shift of the ion front; (ii) the decay of the field into the vacuum is distinctly slower than in the reference case; this is due to the increased mobility of the hot electrons, which carry space charge and consequently electrical field away from the surface; (iii) a second

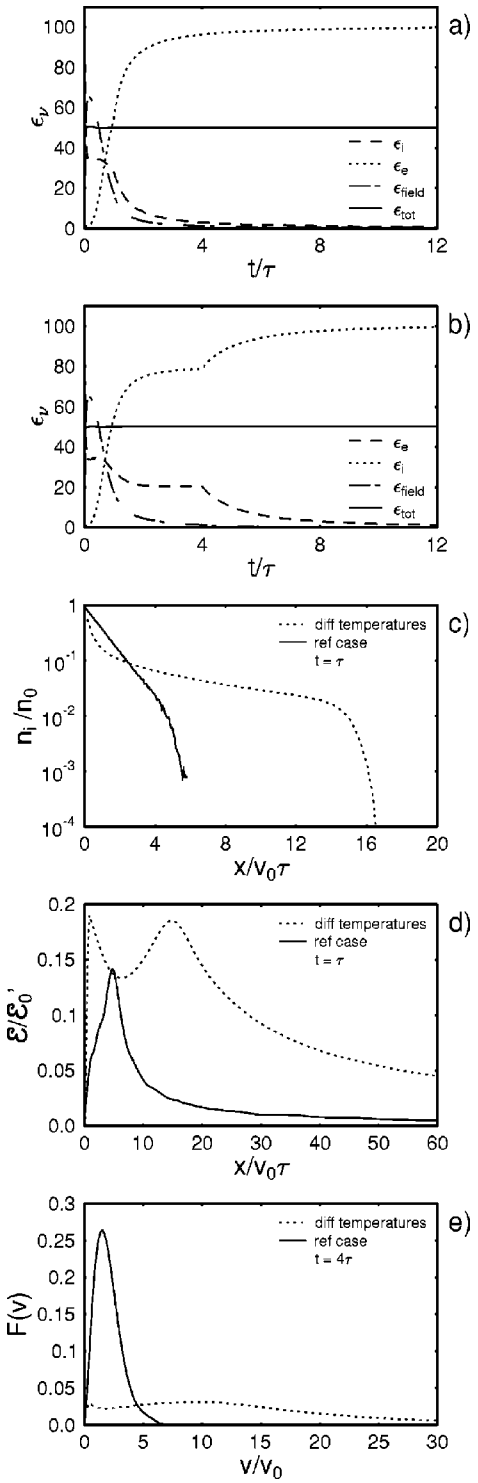

FIG. 5. Characteristics of plasma expansion with a hot electron component. (a) Time evolution of normalized energy per particle, Eq. (4). (b) Analogous to (a), but with a prolonged emission phase continuing until $t=4\tau$. (c) Space dependence of the ion density at time $t=\tau$, compared to the reference case, Fig. 1(b). (d) Space dependence of the electrical field at times $t=\tau$ and $t=4\tau$. The unit of the field $\mathcal{E}_0'$ equals $\mathcal{E}_0$, Eq. (7), for the reference case, but is set to $\tilde{\mathcal{E}}_0$, Eq. (12), for the hot-electron simulation in order to make the field values comparable. (e) Ion velocity distribution, Eq. (9), at time $t=4\tau$, compared to the reference case.

field maximum builds up in the vicinity of the surface. This is due to the vastly different electron and ion speeds, which render plasma neutralization difficult close to the surface.

Figure 5(e) gives the ion velocity spectrum. This figure most clearly shows the very efficient ion acceleration that has happened due to the interaction with the hot-electron cloud.

The prominent result of this simulation is the fact that electrons are able to give their energy very quickly to the ions. This is accomplished by a simple and universal mechanism, i.e., the establishment of a space-charge field. Even drastic energy differences between the electron and ion subsystem are thus quickly equilibrated, such that the energy is transferred almost exclusively to the ion system. Since electrons get their energy easily from the laser field, our simulation exemplifies how, by heating the electron system, energy is quickly transferred to the ionic system.

IV. SUMMARY AND CONCLUSIONS

(1) We investigated the electrostatic mechanism of ion acceleration in the one-dimensional expansion of a plasma off a planar wall into a vacuum. The accelerating electrostatic fields are located mainly at the ion front. Here an electrical double layer is formed as a consequence of the high electron speed that carries electrons far out into the vacuum in front of the ion cloud.

(2) This basic mechanism can be influenced by various plasma processes. We investigate a few of these, concentrating on one at each time.

(3) Ions of different charge state will be accelerated in proportion to their charge. This trivial effect results in a spatial segregation of the different charge states and a stronger acceleration of highly charged ions.

(4) Spatial segregation will also occur in a plasma consisting of a binary mixture of ions with different mass. If both species have been desorbed from the wall with identical temperature, the lighter species will expand more quickly into the vacuum and hence become separated from the heavier species. This spatial segregation will lead to a stronger acceleration of the light species, since the space-charge field is concentrated on the ion expansion front [see item (1) above], and hence on the light species.

(5) If the plasma is not fully ionized, collisions with neutrals will convey part of the ion energy to the neutral system, thus decelerating the ions. This is a frictionlike mechanism, which may eventually lead to an adjustment of ion and neutral velocities, thus counteracting spatial segregation. If ions of different mass, or of different charge state, are present in the plasma cloud, due to the frictionlike interaction with the neutral component, also their respective velocities will assimilate. This effect counteracts the specific acceleration processes mentioned in items (3) and (4) above.

(6) We finally examined the evolution of a plasma cloud, in which the electron component desorbs from the surface with a higher velocity than the ionic component. Due to the strong electrostatic coupling of the two subsystems, energy transfer from the electronic to the ionic system is very efficient and fast. Within a few ten periods of the ion plasma

frequency, the electrons transfer almost all their energy to the ions.

(7) This latter model can be considered as a (rather simplistic) model of plasma expansion due to intense laser interaction with a surface, in which electrons and ions are emitted without being in thermal equilibrium, and the electron energies by far exceed the ion energies.

(8) The simulations presented in this paper are meant to give an overview over processes occurring during plasma expansion. The list of processes included is not complete, and furthermore several of the above mentioned processes can be operative simultaneously. We also note that our simulations describe only the very first phase of plasma expansion, where the expansion can be modeled as one dimensional. Thus, processes occurring later in the flow (at lower plasma density), in a three-dimensional (diverging) flow, or under the interaction with the laser light are excluded from our consideration.

ACKNOWLEDGMENT

Support by the Deutsche Forschungsgemeinschaft is gratefully acknowledged.

[1] T. P. Hughes, *Plasmas and Laser Light* (Hilger, Bristol, 1975).
[2] C. R. Phipps and R. W. Dreyfus, in *Laser Ionization Mass Analysis*, edited by A. Vertes, R. Gijbels, and F. Adams, Chemical Analysis Vol. 124 (Wiley, New York, 1993), p. 369.
[3] D. Bäuerle, *Laser Processing and Chemistry*, 3rd ed. (Springer, Berlin, 2000).
[4] C. Sack and H. Schamel, Phys. Rep. **156**, 311 (1987).
[5] A. Rupp and K. Rohr, J. Phys. D **28**, 468 (1995).
[6] B. Toftmann, J. Schou, T. N. Hansen, and J. G. Lunney, Phys. Rev. Lett. **84**, 3998 (2000).
[7] S. Amoruso, X. Wang, C. Altucci, C. de Lisio, M. Armenante, R. Bruzzese, and R. Velotta, Appl. Phys. Lett. **77**, 3728 (2000).
[8] M. Ye and C. P. Grigoropoulos, J. Appl. Phys. **89**, 5183 (2001).
[9] A. V. Gurevich, L. V. Pariiskaya, and L. P. Pitaevskii, Sov. Phys. JETP **22**, 449 (1966).
[10] Y. A. Bykovskii, N. N. Degtyarenko, V. F. Elesin, V. E. Kondrashov, and E. E. Lovetskii, Sov. Phys. Tech. Phys. **18**, 1597 (1974).
[11] C. K. Birdsall and A. B. Langdon, *Plasma Physics via Computer Simulation* (McGraw-Hill, New York, 1991).
[12] R. W. Hockney and J. W. Eastwood, *Computer Simulation using Particles* (IOP, Bristol, 1994).
[13] C. K. Birdsall, IEEE Trans. Plasma Sci. **19**, 65 (1991).
[14] O. Ellegaard, T. Nedelea, J. Schou, and H. M. Urbassek, Appl. Surf. Sci. **197-198**, 229 (2002).
[15] T. Nedelea and H. M. Urbassek, Phys. Plasmas **9**, 3209 (2002).
[16] J. Denavit, Phys. Rev. Lett. **69**, 3052 (1992).
[17] H. J. Lee and J. P. Verboncoeur, Phys. Plasmas **8**, 3077 (2001).
[18] P. P. Pronko, S. K. Dutta, D. Du, and R. K. Singh, J. Appl. Phys. **78**, 6233 (1995).
[19] G. Bekefi, *Principles of Laser Plasmas* (Wiley, New York, 1976).
[20] *Laser-Induced Plasmas and Applications*, edited by L. J. Radziemski and D. A. Cremers (Dekker, New York, 1989).
[21] L. Landau and E. Lifschitz, *Fluid Mechanics*, Course of Theoretical Physics Vol. 6 (Pergamon, London, 1959).
[22] H. Opower and W. Press, Z. Naturforsch. A **21A**, 344 (1966).
[23] W. Demtröder and W. Jantz, Plasma Phys. **12**, 691 (1969).
[24] L. Torrisi, S. Gammino, L. Ando, and L. Laska, J. Appl. Phys. **91**, 4685 (2002).
[25] A. Thum-Jaeger, B. K. Sinha, and K. P. Rohr, Phys. Rev. E **63**, 016405 (2001).
[26] T. Müller and K. Rohr, J. Phys. D **35**, 352 (2002).
[27] W. H. Cramer, J. Chem. Phys. **30**, 641 (1959).
[28] P. Mulser, Plasma Phys. **13**, 1007 (1971).
[29] R. W. Dreyfus, J. Appl. Phys. **69**, 1721 (1991).